A new treatment of nonadiabatic dynamics: Application to the determination of the He + +H 2 →He+H+H + differential cross section

François Aguillon

Citation: The Journal of Chemical Physics **109**, 560 (1998); doi: 10.1063/1.476592
View online: http://dx.doi.org/10.1063/1.476592
View Table of Contents: http://scitation.aip.org/content/aip/journal/jcp/109/2?ver=pdfcov
Published by the AIP Publishing

A new treatment of nonadiabatic dynamics: Application to the determination of the $He^+ + H_2 \rightarrow He + H + H^+$ differential cross section

François Aguillon
Laboratoire des Collisions Atomiques et Moléculaires (URA du CNRS No. 281), Bâtiment 351, Université Paris XI, 91405 Orsay Cedex, France

(Received 24 November 1997; accepted 3 April 1998)

The dynamics of the dissociative charge exchange reaction $He^+ + H_2(v \leqslant 4) \rightarrow He + H + H^+$ is investigated theoretically at a relative collision energy ranging from 2 eV to 10 eV. Because of the weakness of the nonadiabatic couplings involved in this process, it has been possible to use a new method, which consists in dividing the theoretical treatment in two parts; a semiclassical coupled wave packet method describes the charge exchange between He^+ and H_2, while the dynamics of the dissociation of H_2^+ in the presence of the He atom is handled classically. The time dependent description of the reaction provides a simple interpretation of the strong dependence of the cross section with the collision energy and the initial vibrational excitation of H_2. It is shown that the reaction mechanism is qualitatively different for the different initial vibrational quantum states of H_2. An interesting dynamical effect is observed in the $v = 0$ case; the H^+ ions are scattered primarily in the forward direction relative to the initial H_2 direction, while the neutral H atoms are backward scattered. Moreover, the H^+ ions are on average faster than the neutral H atoms. The results are successfully compared with the available integral and differential experimental data. © *1998 American Institute of Physics.* [S0021-9606(98)02926-2]

I. INTRODUCTION

A large number of experiments[1–12] have been devoted to the study of the dissociative charge exchange (DCE) between He^+ and H_2,

$$He^+ + H_2(v) \rightarrow He + H + H^+ \tag{1}$$

at center of mass collision energies above 1 eV. When the hydrogen atom is produced in an optically active excited state, the experimental measurements of the integral cross sections based upon the detection of its fluorescence[4,8–12] are in fair agreement.[13] When the collision energy is below 10 eV, the hydrogen atom is mainly produced in its ground state; absolute cross sections measurements are more difficult, and the available data are not in mutual agreement.[13] In the eV energy range however, the situation becomes much simpler from a theoretical point of view, all the excited states of the HeH_2^+ system can be disregarded, except of course the states correlated to the reactants $He^+(1s) + H_2(X\ ^1\Sigma_g^+)$ and the products $He(1s^2) + H_2^+(^2\Sigma_u^+)$, thereafter denoted $|1\rangle$ and $|2\rangle$, respectively. The ground state thereafter denoted $|3\rangle$ is correlated to $He(1s^2) + H_2^+(^2\Sigma_g^+)$. It is not expected to interact with the reactants state, but is coupled to the state $|2\rangle$ at large H–H distance.[14–16]

A large amount of work has been devoted to the calculation of the potential energy surfaces (PES) of this system.[17–29] High accuracy fits of the three lowest adiabatic states of the HeH_2^+ system have been obtained by Aguado *et al.*[30] from *ab initio* potentials of 596 nuclear configurations computed by McLaughlin and Thompson.[28] Despite this good knowledge of the PES, the theoretical calculation of the cross section of reaction (1) is not easy. Indeed, on one hand, two purely quantal effects play an essential role in the dynamics of this DCE process, the nonadiabatic effects, of course, and a very important tunneling.[27] On the other hand, the problem appears to be much too complicated to be completely handled by quantum mechanics, especially because one should deal not only with the continuum associated with the collision motion, but also with the continuum associated with the dissociation of the H_2^+ ion.

In a previous publication,[31] a semiclassical coupled treatment[32,33] has been used to determine the integral cross section of the title reaction. The main advantage of this method is its ability to handle the above mentioned nonadiabatic transitions and tunneling effects, while it keeps the amount of calculation to a very reasonable size by handling quantally only one degree of freedom, namely the H–H distance. However, the common trajectory approximation[34] made in this implementation of the semiclassical approximation makes this method inadequate to provide reliable differential results. Indeed, as the orientations of the H and H^+ velocity vectors at the end of the collision strongly depend on the orientation of the H_2 axis before the dissociation, differential calculations require a precise determination of the H_2 rotation motion. This rotation motion strongly depends on whether the molecule dissociates or not. Thus, it cannot be accurately described by a common trajectory approach.

The basic idea of the present work is to avoid this difficulty by treating the collision in two stages; the first one concerns the charge transfer between the He^+ ion and the H_2 molecule. It makes use of the semiclassical coupled wave packet treatment. The second stage deals with the dissociation of H_2^+ in the presence of He, and especially with the sharing of the electric charge between the two H atoms. It involves purely classical dynamics. One should emphasize

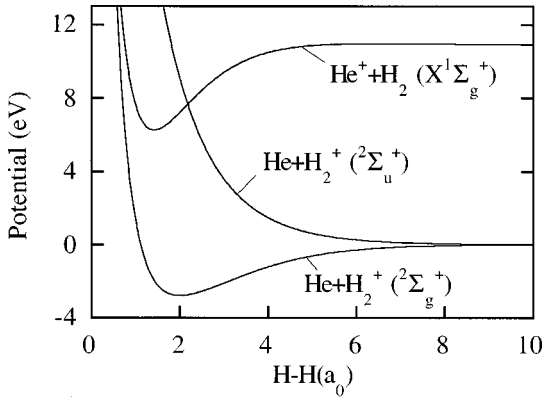

FIG. 1. Asymptotic potential energy curves of the $(He+H_2)^+$ system.

that using such a two stage treatment does not mean at all that the collision is described within a sudden approximation where the charge transfer is assumed to take place at a fixed position. Such an approximation would not be valid in the energy range studied here. On the contrary, the transition between the semiclassical treatment and the classical treatment is progressive, in the sense that it can last as long as a few vibrational periods of H_2. The detailed description of this method together with the justification of the approximations will be presented in the first section of this paper. In the second section, the results are presented and related to the mechanisms of the dissociative charge exchange. Finally, the third section presents the comparison of the results with previously published data.

II. DYNAMICAL TREATMENT

As long as the collision energy is not too high, only the three electronic states $|1\rangle$, $|2\rangle$, and $|3\rangle$, are involved in the process studied here (Fig. 1). One important characteristic of this system is that the couplings responsible for the nonadiabatic transitions are very weak. The coupling between states $|1\rangle$ and $|2\rangle$ is weak essentially because these electronic states differ by two orbitals one electron of the H_2 molecule goes to the He atom, and the other electron goes from the σ_g to the σ_u orbital.[35] The coupling between states $|2\rangle$ and $|3\rangle$ is weak because it results from the interaction of H_2^+ with a helium atom in its almost inert $(1s^2)$ ground state. Then, transitions can occur only in regions where the coupled states are energetically very close to each other. Consequently, the DCE process involves two distinct nonadiabatic transitions; the $|1\rangle \rightarrow |2\rangle$ transition occurs near the equilibrium distance of H_2, and the $|2\rangle \rightarrow |3\rangle$ transition occurs at very large H–H distance. The theoretical treatment used here exploits these features, by describing the DCE process as two successive two state problems. The first part of the theoretical treatment is devoted to the study of the $|1\rangle \rightarrow |2\rangle$ transition

$$He^+ + H_2 \rightarrow He + H_2^+(^2\Sigma_u^+). \tag{2}$$

This part determines the integral DCE cross section. The differential cross sections are obtained in the second part of the calculation, which deals with the dissociation of H_2 in the presence of the He atom,

$$He + H_2^+(^2\Sigma_u^+) \rightarrow He + H + H^+. \tag{3}$$

It is important to note that the numerical efforts required for each of these two parts are very different. Indeed, for the $|1\rangle \rightarrow |2\rangle$ transition there is a strong coupling between the electronic state of the system and the vibrational motion of the H_2 molecule; a change of electronic state strongly affects the nuclear motion. Conversely, as the $|2\rangle \rightarrow |3\rangle$ transition occurs at very large H–H distance between electronic states which are quasidegenerate with respect to the dissociation energy, it does almost not affect the dissociation motion. Then, the dynamics is not treated in the same way for the two reactions (2) and (3). For the study of (2), both the electronic motion and the relative H–H motion are handled quantally using a semiclassical approach. For the study of (3), only the electronic motion is handled quantally, while the dynamics is purely classical. Obviously, one problem that must be solved is the linking of the two parts of the calculation, essentially because the H–H coordinate is handled quantally at the beginning of the process, and classically at the end.

A. First stage

The theoretical treatment of reaction (2) is based upon a coupled wave packet method.[33] The total wave function $\Xi(\mathbf{r},\mathbf{R},\boldsymbol{\rho})$ of the HeH_2^+ system depends on the Jacobi vector $\mathbf{r}$ joining the two H atoms, on the Jacobi vector $\mathbf{R}$ joining the He atom to the center of mass of the H_2 molecule, and on the electronic coordinates, collectively denoted by $\boldsymbol{\rho}$. The wave function can then be expanded over a diabatic electronic basis set (see Ref. 35, and references therein),

$$\Xi(\mathbf{r},\mathbf{R},\boldsymbol{\rho}) = \Phi_1(\mathbf{r},\mathbf{R})|1\rangle + \Phi_2(\mathbf{r},\mathbf{R})|2\rangle. \tag{4}$$

In order to make the calculation tractable, it is necessary to reduce the number of quantal degrees of freedom of the wave functions Φ_1 and Φ_2. This is done by treating classically the collision motion $\mathbf{R}(t)$ and the H_2 rotation motion $\hat{r}(t)$. Then, only the vibrational motion of H_2 is handled quantally. The time dependent Schrödinger equation leads to a set of coupled differential equation involving the radial H–H part φ_i of the nuclear wave functions Φ_i appearing in Eq. (4),

$$\begin{cases} i\hbar \dfrac{\partial \varphi_1(r,t)}{\partial t} = T\varphi_1(r,t) + H_{11}\varphi_1(r,t) + H_{12}\varphi_2(r,t) \\ i\hbar \dfrac{\partial \varphi_2(r,t)}{\partial t} = T\varphi_2(r,t) + H_{22}\varphi_2(r,t) + H_{21}\varphi_1(r,t). \end{cases} \tag{5}$$

T is the kinetic energy operator associated with the radial motion H–H; H_{ij} are the matrix elements of the electronic Hamiltonian, which depends on time via the classical trajectory $\hat{r}(t)$, $\mathbf{R}(t)$,

$$H_{ij}(r,\hat{r},\mathbf{R}) = \langle i|H_{el}(r,\hat{r},\mathbf{R})|j\rangle, \tag{6}$$

where the integration is carried out over the electronic coordinates. The H_{ij} matrix elements used are those obtained by Aguado *et al.*[30]

One important problem in the semiclassical approximation is the determination of the classical trajectory.[34] The first work on this system[31] used (i) the frozen rotor

approximation[36,37] for the $\hat{r}(t)$ motion, and (ii) the semiclassical energy conserving common trajectory (SCECT) (Refs. 34, 38, 39) method to determine the collision motion $\mathbf{R}(t)$, governed by the Hamiltonian,

$$H_{\text{class}}(\hat{r},\mathbf{R})=\sum_{i,j}\int \varphi_i^*(r,t)H_{ij}(r,\hat{r},\mathbf{R})\varphi_j(r,t)dr. \quad (7)$$

In the present work, a different choice of trajectory has been made; both the $\mathbf{R}(t)$ and the $\hat{r}(t)$ motions are governed by the classical Hamiltonian,

$$H_{\text{class}}(\hat{r},\mathbf{R})=H_{11}(\langle r_1\rangle,\hat{r},\mathbf{R}), \quad (8)$$

where $\langle r_1\rangle$ is the expectation value of the r coordinate in the electronic state 1. This choice is motivated by three reasons.

(i) The goal of this stage of the calculation is to give an accurate description of the process *before* the dissociation takes place; the description of the dissociation itself is done in the second stage of the calculation. During this first stage, the system is in the state $|1\rangle$, whose evolution is essentially governed by H_{11}. The classical Hamiltonian (8) is then better suited to that aim than the classical Hamiltonian (7).

(ii) An accurate description of the rotation of H_2 requires us to go beyond the frozen rotor approximation.

(iii) Because the average along the r coordinate is not performed in the same way, the Hamiltonian (8) leads to a smaller amount of computation than (7). Indeed, using (7) leads to evaluate at each time step the space derivatives of the H_{ij} matrix elements all over the r range. The advantage of this time consuming r-averaging is that it ensures a perfect conservation of the expectation value of the energy.[34,38,39] As soon as an alternative classical Hamiltonian is used, this advantage does not hold any more. It is then consistent to use a cheaper r-averaging, as the one performed in (8).

The quantal set of equations (5) is solved numerically by expanding the wave packets $\varphi_i(r,t)$ over a grid. The action of the kinetic energy operator is evaluated by the FFT technique.[40,41] An important effort had to be made to reduce the computational effort needed for the evaluation of the H_{ij} matrix (6). This matrix has to be calculated at each time step all over the r grid at the current values of the Jacobi coordinates $R(t)$ and $\gamma(t)$, which is the $(\mathbf{r},\mathbf{R})$ angle. In order to save computation time, this evaluation is performed by using at each time step the numerical fit of Aguado *et al.*[30] at a few points (typically 15) r_i, $R(t)$, $\gamma(t)$; a cubic spline interpolation is performed between the r_i. This requires the choice of the r_i abscissas of the spline points to be chosen dynamically, since in the near collinear geometry, the potential exhibits a (time dependent) singularity at $r=2R(t)$. The time evolution of the vibrational wave packets $\varphi_i(r,t)$ is handled by the short iterative Lanczos procedure.[42] Simultaneously, Hamilton's classical equations governing the classical motion are solved using a fourth order Runge Kutta integrator. At each collision energy and for each initial vibrational quantum number v of H_2, the initial conditions are sampled over $n_{\text{orient}}=32$ initial orientations of the H_2 axis and typically 30 impact parameters, resulting in typically $N_{\text{sc}}=960$ so-called semiclassical trajectories, i.e., N_{sc} $\{\mathbf{R}(t),\hat{r}(t)\}$ trajectories describing the time evolution of the degrees of freedom which are handled classically in the semiclassical approximation. In most of the calculations, the size of the grid has been maintained to a relatively small value (typically $10a_0$), and the outermost part of the dissociating wave packet has been removed from the grid in order to avoid reflection at the edge of the grid. A few calculations have been done on a large grid, in order to analyze the dissociative wave packet by projection onto the continuum eigenstates of the H_2^+ $^2\Sigma_u^+$ ion.

B. Second stage

The wave packet calculation of the first stage of the DCE process (2) provides the vibronic state-to-state integral cross sections. It also provides some information on the time evolution of the DCE process. The basic idea of the method proposed here is to use these informations to determine when during the collision the $|1\rangle\rightarrow|2\rangle$ transition takes place, and what is the dynamical state of the system when this transition occurs. Just in the same way as in the trajectory surface hopping method,[43] the system is then supposed to be entirely in the state $|2\rangle$ just after the transition and to evolve classically. The link between the semiclassical part of the calculation and the purely classical one must take into account the fact that in the energy range studied here, the dissociation takes place *during* the collision. The part of the wave packet which performs the $|1\rangle\rightarrow|2\rangle$ transition at the beginning of the collision does not see the same potential during the dissociation stage as the part of the wave packet which performs the $|1\rangle\rightarrow|2\rangle$ transition at the end of the collision, since the position of the He atom is different. In order to take this into account, each semiclassical calculation, characterized by the initial value b_k of the impact parameter and the initial orientation $\hat{r}_k$ of H_2 $(1\leqslant k\leqslant N_{\text{sc}})$, gives rise in the second stage of the theoretical treatment to n_k classical trajectories, in such a way that the n_k sets of initial conditions are as representative of quantal behavior of the system as possible.

The first step is to determine the number n_k of classical trajectories associated to each of the N_{sc} semiclassical samples $\{b_k,\hat{r}_k\}$. This number must reflect the weight of the semiclassical sample k in the integral cross section. Then, the n_k are determined by

$$n_k=\frac{b_k P_2(b_k,\hat{r}_k,t\rightarrow\infty)}{\sum_{k'=1}^{N_{\text{sc}}} b_{k'}P_2(b_{k'},\hat{r}_{k'},t\rightarrow\infty)}N, \quad (9)$$

where N is the total number of classical trajectories launched. In the present work, N has been set to 10 000. Note that in order to solve this equation, one first has to complete the semiclassical calculation of the N_{sc} semiclassical samples up to the end of the collision.

For the sake of clarity, the procedure governing the determination of the n_k classical trajectories associated to each of the semiclassical samples $\{b_k,\hat{r}_k\}$ will first be presented having in mind a prototype case characterized by an extremely weak value of the H_{12} coupling. In such an ideal situation, the $|1\rangle\rightarrow|2\rangle$ transition can only take place at the

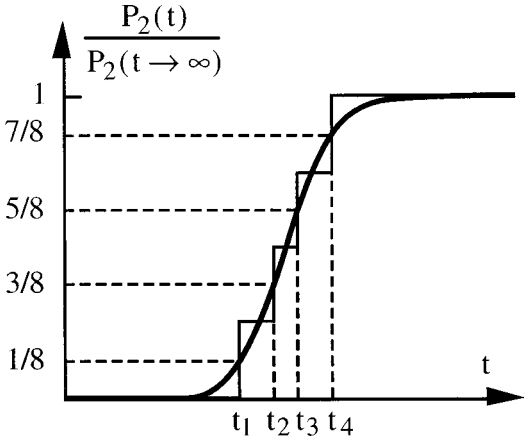

FIG. 2. Bold line, typical time evolution of the state 2 population P_2 during reaction (2). If four trajectories are to be launched for the classical calculation of reaction (3), the associated transition times t_j are chosen in such a way that they account for the time evolution of P_2, as indicated by the thin line.

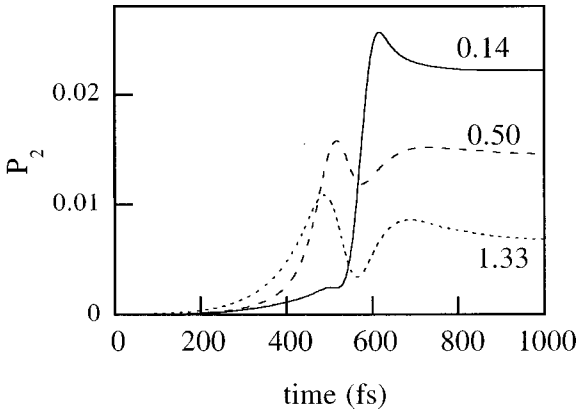

FIG. 3. Three examples of time evolution of the state 2 population P_2 in actual cases. The value of the function f_{osc} which evaluates the degree of oscillations is reported on each curve.

crossing seam, and the behavior of the system is essentially perturbative. Consequently, the time evolution of the state $|2\rangle$ population, as determined by the semiclassical approximation,

$$P_2(b_k,\hat{r}_k,t)=\langle\varphi_2(t)|\varphi_2(t)\rangle \tag{10}$$

is very likely to look like the function represented in Fig. 2, i.e., is a monotonously increasing function of time. To account for the duration of the $|1\rangle\rightarrow|2\rangle$ transition, the basic idea is to launch the n_k classical trajectories at different transition time t_{jk}, $1\leqslant j\leqslant n_k$, in such a way that the time evolution of the state $|2\rangle$ population during the second stage follows as closely as possible the time dependence of $P_2(b_k,\hat{r}_k,t)$. As seen in Fig. 2, this prescription leads to choose the t_{jk} such that

$$P_2(b_k,\hat{r}_k,t_{jk})=\frac{j-1/2}{n_k}\,P_2(b_k,\hat{r}_k,t\rightarrow\infty). \tag{11}$$

Once again, one can note that in order to solve this equation, one has to complete the semiclassical calculation up to the end of the collision.

As mentioned before, the classical calculation assumes that the system is in the state $|2\rangle$ at $t=t_{jk}$. Its dynamical state is deduced from the calculation of the first stage; $\mathbf{R}$, $\hat{r}$ and the associated momenta are known from the semiclassical calculation. The value of $r(t_{jk})$ is fixed by the property that the transition takes place exactly at the crossing $r_x(\hat{r},\mathbf{R})$ between states $|1\rangle$ and $|2\rangle$. The last unknown initial dynamical quantity is the momentum $p_r(t_{jk})$ associated to the radial motion of H_2. It is fixed using the energy conservation,

$$p_r^2=2\mu(E_{\mathrm{tot}}-E_{\mathbf{R}}-E_{\hat{r}}-H_{22}(r_x(\hat{r},\mathbf{R}),\hat{r},\mathbf{R})), \tag{12}$$

where E_{tot} is the total energy, H_{22} is the potential, $E_{\mathbf{R}}$ is the kinetic energy associated with the $\mathbf{R}$ motion, $E_{\hat{r}}$ is the kinetic rotation energy of the hydrogen molecule, and μ its reduced mass.

Before going further, it is necessary to examine the validity in actual cases of three assumptions which have been done above in the above presentation of the prototype case. The first assumption is that $P_2(b_k,\hat{r}_k,t)$ is a monotonously increasing function of the time; the splitting of the calculation in two parts is based on the neglect of multiple $|1\rangle\leftrightarrow|2\rangle$ transitions. If this assumption is wrong, then $P_2(b_k,\hat{r}_k,t)$ will present oscillations. A function f_{osc}, defined by

$$f_{\mathrm{osc}}(k)=\frac{1}{\max(P_2(b_k,\hat{r}_k,t))}\int\left|\frac{dP_2(b_k,\hat{r}_k,t)}{dt}\right|dt-1 \tag{13}$$

has been used to measure the degree of oscillation of $P_2(t)$. One easily checks that f_{osc} vanishes if $P_2(t)$ is strictly monotonously increasing; $f_{\mathrm{osc}}=1$ if P_2 increases from 0 to its maximum value, and decreases back to zero; $f_{\mathrm{osc}}=2$ if P_2 increases from 0 to its maximum value, then decreases back to zero, and increases once again to its maximum value. Figure 3 shows three examples of evaluation of f_{osc} in actual cases. At a given collision energy E_{col} and a given initial vibrational number v, the oscillation rate is reflected by $\langle f_{\mathrm{osc}}\rangle$, obtained by weighting the contribution of the N_{sc} semiclassical $\{b_k,\hat{r}_k\}$ samples according to their contribution to the DCE cross section,

$$\langle f_{\mathrm{osc}}\rangle=\frac{\Sigma_{k=1}^{N_{\mathrm{sc}}}f_{\mathrm{osc}}(k)b_kP_2(b_k,\hat{r}_k,t\rightarrow\infty)}{\Sigma_{k=1}^{N_{\mathrm{sc}}}b_kP_2(b_k,\hat{r}_k,t\rightarrow\infty)}. \tag{14}$$

In most of the situations, $\langle f_{\mathrm{osc}}\rangle$ is found to be rather low. For example, at $E_{\mathrm{coll}}=5$ eV, it ranges between 0.0112 for $v=3$ and 0.278 for $v=0$. It does never exceed 50%, except at $v=0$ below $E_{\mathrm{coll}}=4$ eV; besides, these situations correspond to very small DCE cross sections. Nevertheless, the fact that $P_2(t)$ is not strictly monotonous makes the use of Eq. (11) impossible. Then, the determination of the transition times t_{jk} has been done according to the following rule:

$$P_2(b_k,\hat{r}_k,t_{jk})=P_2(t_-)+\frac{j-1/2}{n_k}\,(P_2(t_+)-P_2(t_-))$$

$$t_-\leqslant t_{jk}\leqslant t_+, \tag{15}$$

where t_- is the time of the last extremum of $P_2(b_k,\hat{r}_k,t)$ reached before the turning point, and t_+ the time of the first

extremum of $P_2(b_k,\hat{r}_k,t)$ reached after the turning point. Equation (15) cannot be justified from first principles. When $P_2(t)$ is monotonous, it is strictly equivalent to Eq. (11), and provides a uniform sampling of the transition. In the few cases when oscillations show up in the $P_2(t)$ function, it tends to locate the transition near the turning point of the trajectory, i.e., near the place where the transition rate is expected to be maximum.

The second assumption which has been done in the presentation of the prototype case if the localization of the transition at the crossing seam. The validity of this strong assumption can be checked by the wave packet calculation; the width of transition region has been estimated by running a test wave packet calculation on a PES with the coupling forced to be zero in a region Δr_x around the crossing seam. The test has been done for $E_{\rm coll}=5$ eV, $v=0$; the initial conditions b and $\hat{r}$ are those which give the largest contribution to the cross section. The DCE probability is divided by two when Δr_x is as small as $0.06\,a_0$, and by four when $\Delta r_x=0.15\,a_0$. This shows that the localization of the transition on the crossing seam is a very good approximation if the case studied here.

Finally, it has been implicitly assumed that there is always one solution to Eq. (12). Actually, this is never the case. Indeed, if the crossing seam lies in the classically allowed region, there are two solutions, one negative and one positive. In such a situation, the trajectory is launched with p_r alternatively positive and negative. On the other hand, if the crossing seam lies out of the classically allowed region, p_r^2 as given by Eq. (12) is negative. In such a situation where the transition takes place by tunneling, the classical calculation is launched with $p_r=0$, and the energy is not conserved. The final energy provides then another test of the validity of the method. The total energy averaged over all the trajectories is conserved within less than 0.2 eV at $v=0$, except below $E_{\rm coll}=4$ eV, where the tunneling effect plays an important role. The energy conservation is perfect for $v\geqslant 3$.

Once the initial dynamical conditions of the second stage of the calculation are determined, the motion of the nuclei on the PES associated with the electronic states $|2\rangle$ and $|3\rangle$ can be calculated. This latter state is involved in the process since near the He atom, the H_2^+ *gerade* and *ungerade* state are coupled together. This H_{23} coupling is responsible for the localization of the electric charge on one of the two H atoms at the end of the collision. In a study of collision induced dissociation between He and H_2^+, Gislason *et al.*[14–16] have shown that this localization of the electric charge takes place at rather large r value. Then, it should not affect the *relative* motion of the H atoms, which can be determined on the PES of the state $|2\rangle$. Nevertheless, the final positions and velocities of the H^+ ion and of the H atom in the center of mass frame depend obviously on the localization of the electric charge. In order to determine the charge sharing, the state of the system is described as

$$\psi(t)=A(t)|a\rangle+B(t)|b\rangle, \tag{16}$$

where $|a\rangle$ and $|b\rangle$ are the diabatic electronic states correlated with $He+H_a^++H_b$ and $He+H_a+H_b^+$. The time evolution of a and b is given by

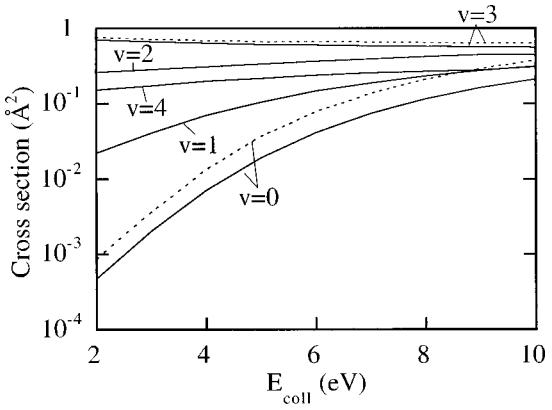

FIG. 4. Dissociative charge exchange cross section between He^+ and H_2 as a function of the center of mass collision energy $E_{\rm coll}$ and the initial vibrational quantum number v of the hydrogen molecule. Full lines, present work; dotted lines, results obtained in the frozen rotor approximation (Ref. 31).

$$\begin{cases} i\hbar\dot{A}=H_{aa}A+H_{ab}B \\ i\hbar\dot{B}=H_{ba}A+H_{bb}B, \end{cases} \tag{17}$$

where the matrix elements H_{xy}, defined by

$$H_{xy}(\mathbf{r},\mathbf{R})=\langle x|H_{\rm el}(\mathbf{r},\mathbf{R})|y\rangle \tag{18}$$

depend on time via the classical motion. The initial value of A and B are set by the condition that the initial electronic state is the state $|2\rangle$, which is the excited adiabatic state obtained by diagonalizing the electronic Hamiltonian in the $\{|a\rangle,|b\rangle\}$ basis set. As the transitions occur at very large H–H distance, this diabatic Hamiltonian has been simply evaluated by the DIM expression of Whitton and Kuntz[20] modified by Sizun and Gislason[16] to account for the polarization of the He atom by the H_2^+ ion.

III. RESULTS AND INTERPRETATION

A. Integral cross section

The integral cross section $\sigma_{\rm DCE}$ of reaction (1) has been calculated for center of mass collision energies lying between 2 and 10 eV, and for the initial vibrational states of the hydrogen molecule $v=0$ to $v=4$ (Fig. 4). As reported in Ref. 31, several striking features can be noted.

(i) for $v=0$, $\sigma_{\rm DCE}$ increases by more than two orders of magnitude between 2 and 10 eV. This increase is less pronounced for $v=1$, 2 or 4. The $v=3$ level is peculiar, since its cross sections decreases when the collision energy increases;

(ii) at $E=2$ eV, a strong vibrational enhancement of the $\sigma_{\rm DCE}$—three orders of magnitude—is observed up to the $v=3$ level. This enhancement is less pronounced when the energy increases. One can note that such a vibrational enhancement of the dissociative charge exchange has also been reported at thermal energies.[27,44]

The two above mentioned enhancements of $\sigma_{\rm DCE}$, either translational or vibrational, do not have the same origin at

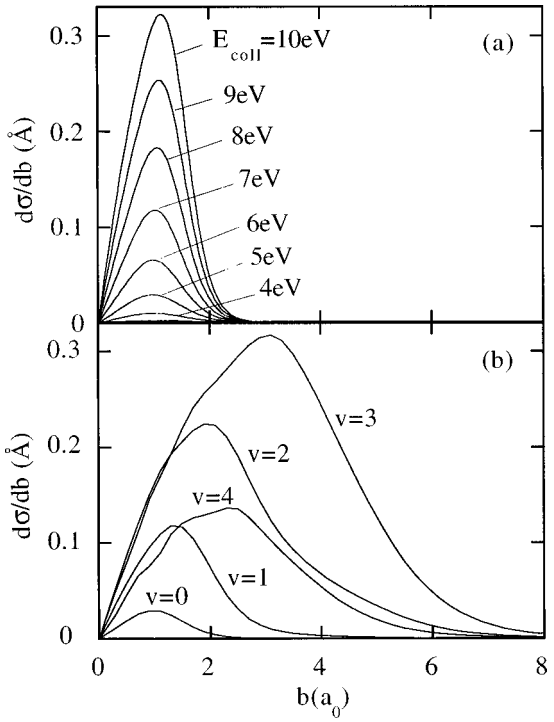

FIG. 5. Contribution of the different impact parameters b to the DCE cross section. Frame (a): $v=0$. Frame (b): $E_{\mathrm{coll}}=5$ eV.

all. This is witnessed by Fig. 5, which represents the contribution of the different impact parameters to the integral DCE cross section, defined by

$$\frac{d\sigma_{\mathrm{DCE}}}{db}=\frac{\int 2\pi b P_2(b,\hat{r},t\rightarrow\infty)d\hat{r}}{\int d\hat{r}}. \tag{19}$$

This figure shows that the $v=0$ DCE process always takes place at short intermolecular distance, but is most probable at high collision energy. Conversely, the vibrational dependence of the low energy cross section is clearly due to a variation of the intermolecular distance where the DCE process takes place. That is the reason why in the following we shall focus our attention either on the $v=3$ case, typical of a distant mechanism, or on the $v=0$ process, typical of the short range mechanism.

As mentioned above, the DCE *integral* cross section is entirely governed by the charge exchange between He^+ and H_2 during the first step of the reaction. Then, the interpretation of the above results does not involve the electronic state $|3\rangle$. Three important characteristics of the H_{11}, H_{22}, and H_{12} terms of PES [Figs. 6(b) and 6(c)] explain the results of Figs. 4 and 5. First, the H_{12} coupling term is weak, and thus efficient only in the immediate vicinity of the crossing seam. Second, this crossing seam $r_x(R)$ is such that $r_x(R)<r_x(R\rightarrow\infty)\approx 2.2$ a.u. [Fig. 6(a)]. Third, the H_{11} entrance potential is repulsive along the R coordinate.

At *low collision energy* (typically $E_{\mathrm{coll}}<3$ eV), the repulsive character of H_{11} prevents the system to explore small R regions; therefore, $r_x(R)\approx r_x(R\rightarrow\infty)\approx 2.2\ a_0$ throughout the collision. The DCE is governed by the probability for H_2 to reach such a large elongation, which strongly depends on the vibrational state of H_2 [Fig. 6(d)]. For the $v=0$ state, this

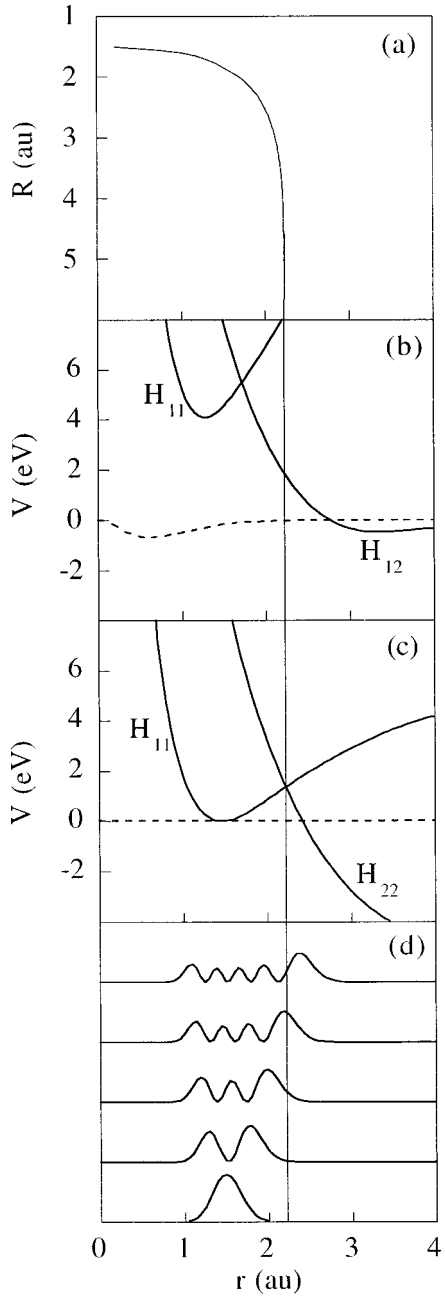

FIG. 6. Frame (a): Location of the crossing seam in the (R,r) plane for $\gamma=30°$. Frame (b): cuts of the diabatic potential matrix elements along the r coordinate for $\gamma=30°$, and $R=2.5a_0$; H_{11} and H_{22} (full lines), $H_{12}\times 10$ (dashed line). Frame (c): same as frame (b), except that $R=8.0\ a_0$. Frame (d): probability densities associated with the first five vibrational eigenstates of H_2.

probability is very weak, and the nonadiabatic transition is very difficult. Conversely, the $v=3$ probability density is large near $r\approx 2.2\ a_0$, leading to a large DCE cross section. At *higher collision energy* (typically $E_{\mathrm{coll}}>5$ eV), the strong enhancement of the $v=0$ DCE cross section is related to the ability for the system to explore small $r_x(R)$ at small R. Since whatever is the value of R the crossing seam is located within the wave packet width, no energetic enhancement of this sort is observed in the $v=3$ case.

Figure 7 shows the dissociation energy spectrum, i.e., the quantity $d\sigma_{\mathrm{DCE}}/dE_{\mathrm{diss}}$, where E_{diss} is the relative kinetic

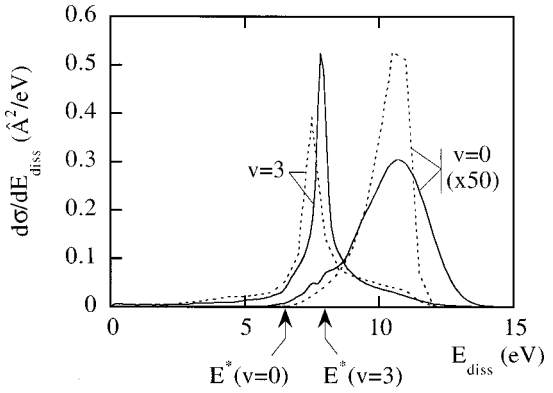

FIG. 7. Dissociation energy spectrum at $E_{\rm coll}=5$ eV, $v=0$ and $v=3$. The full line is the result of the coupled wave packet calculation. The dashed line is the result of the classical calculation. The arrows indicate the position of the resonant dissociation energy $E^*(v)$ defined in (22).

energy of the H and H^+ fragments, irrespective of their flight direction. This spectrum, obtained by projecting the final wave packet φ_2 on the dissociative eigenstates of $H_2^+(2p\sigma_u)$, reflects the difference between the long range and short range mechanisms. Since (i) in the collision energy range studied here the H_2 molecule performs several vibrations during the collision and (ii) the H_{12} coupling is weak, the $|1\rangle \rightarrow |2\rangle$ transition is likely to be a horizontal transition;[45] the dissociation energy is near $E_{\rm hor}$ (Fig. 8) defined by

$$E_{\rm hor}=E_{\rm vib}+H_{11}(R^{\#},\gamma^{\#},r_{\rm eq}(R^{\#},\gamma^{\#})) - H_{22}(R^{\#},\gamma^{\#},r\rightarrow\infty), \tag{20}$$

where $E_{\rm vib}$ is the vibrational energy of the molecule, $r_1^{\rm eq}$ is the equilibrium position of H_2 in the state $|1\rangle$, and $R^{\#}$ and $\gamma^{\#}$ are the respective values of R and γ where the transition takes place. Actually, $R^{\#}$ and $\gamma^{\#}$ do not have an unique value, but cover the transition region. In the $v=3$ case, the main contribution to the DCE integral cross section arises from large $R^{\#}$ values; then, as observed in Fig. 7, the horizontal transition populates the resonant level $E^*(v=3)$, defined by

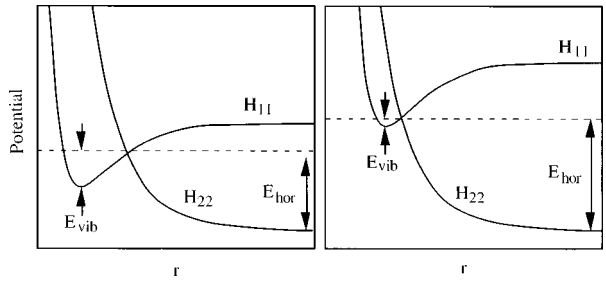

FIG. 8. Scheme of the relative position of the potential energy curves at large R (left) and small R (right). The charge exchange is efficient when the vibronic energy of the system (dashed line) is close to the energy of the crossing point. This occurs at large R for the high v levels, and at small R for the low v levels. It is seen that the horizontal dissociation energy is smaller when v is large.

$$E^*(v)=E_{1v}+\lim_{R\rightarrow\infty}(H_{11}(R,r=r_1^{\rm eq})-H_{22}(R,r\rightarrow\infty)), \tag{21}$$

where E_{1v} is the vibrational energy of the molecule in its eigenstate v. At low v, $R^{\#}$ is small. As the state 1 is more repulsive than the state 2, $H_{11}-H_{22}$ is larger at small R than at large R. Then, as predicted by the local complex potential approximation,[45] the dissociation energy is significantly higher than the resonant energy (Fig. 7). Paradoxically, Fig. 7 also shows that the mean dissociation energy is higher when starting from a $v=0$ level than from a $v=3$ level.

One has to mention the dissociation energy spectrum obtained by projecting the final wave packet φ_2 on the dissociative eigenstates of $H_2^+(2p\sigma_u)$ suffers from a strong approximation. Indeed, as mentioned in the previous section, the Hamiltonian (8) which governs the classical trajectory involved in the semiclassical wave packet calculation, has been designed to give an accurate description of the process before the dissociation takes place. It is not expected to provide accurate results in the description of the dissociation, essentially the $\hat{r}(t)$ motion is quite dependent on the H–H bond length. To overcome this difficulty, one can obtain the H–H dissociation energy spectra from a statistical analysis of the trajectories obtained in the second stage of the calculation. Indeed, the purely classical calculation is much better suited to describe the dissociation. On the other hand, classical mechanics fails to account for any coherence effect during the nonadiabatic transition itself, and thus can barely account for a horizontal transition. The comparison between these completely different methods can be considered as a test of the accuracy of the approximation; it is much better in the $v=3$ case than in the $v=0$ case. This has to be related to the fact that tunneling is much more important at low v than at large v.

B. Differential cross section

The differential results are obtained at the end of the second part of the calculation. In the following will be presented doubly differential cross section $I(\chi,u)$ for the products He, H^+, and H. χ is the center of mass scattering angle of He (respectively, H^+ or H), i.e., the angle between the final velocity vector of He (respectively, H^+ or H) and the initial velocity vector of He^+; u is the final velocity of the He atom (respectively, H^+ or H). This $I(\chi,u)$ function represents the probability to detect the considered particle in the angular range χ, $\chi+d\chi$ and in the velocity range u, $u+du$. It is related to the total cross section $\sigma_{\rm DCE}$ by

$$\sigma_{\rm DCE}=\int_0^{\pi}d\chi\int_0^{\infty}du\;\; I(\chi,u). \tag{22}$$

For each classical trajectory, the deflection angle χ_a of the H_a atom, its final velocity u_a, and its electric charge $|A(t\rightarrow\infty)|^2$ are determined. This trajectory contributes both to the doubly differential cross section $I_{H^+}(\chi_a,u_a)$ for the formation of H^+ with the weight $|A(t\rightarrow\infty)|^2$, and to the doubly differential cross section $I_{\rm H}(\chi_a,u_a)$ for the formation of neutral H with the weight $1-|A(t\rightarrow\infty)|^2$. The same hold of course for the H_b atom.

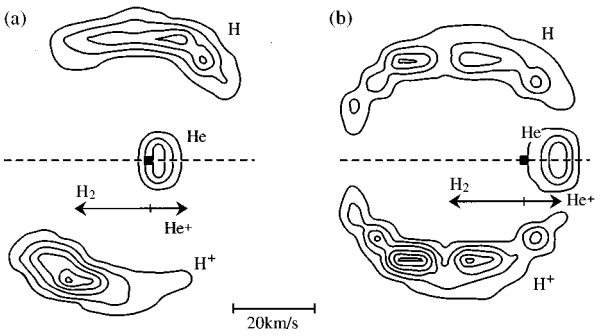

FIG. 9. Contour plot of the doubly differential cross section $I(\chi,u)$ for reaction (1). Left view, $E_{\text{coll}}=5$ eV and $v=0$. Right view, $E_{\text{coll}}=5$ eV and $v=3$. The black square is the origin of the coordinates. The two arrows indicate the initial velocity of He^+ and H_2. Three structures can be seen; the He corresponds to the sharp peak on both sides of the dashed line; the two broad structures lying above and below this dashed line correspond to the neutral H and to H^+, respectively. Note that for sake of clarity, the distance between two successive contour lines has been chosen larger in the He peak than in the hydrogen peaks.

Figure 9 shows the doubly differential cross section $I(\chi,u)$ obtained in such a way. At $E_{\text{coll}}=5$ eV in the $v=0$ case [Fig. 9(a)], it is seen that the H and H^+ atoms are preferentially scattered at a deflection angle χ around 90°. This nonuniform distribution is partly due to the representation chosen here, where the volume element is $d\chi$ instead of the usual $\sin\chi d\chi$. Nevertheless, this jacobian effect is not sufficient to explain the angular distribution of H and H^+; the function $I(\chi,u)/\sin\chi$ is also preferentially localized around 90°. This nonuniformity of the *final* orientation of the H–H axis has to be related to the non uniformity of the DCE cross section with respect to the initial orientation of H_2. In the following, the initial direction of the collision velocity vector will be denoted Oz, and the initial triatomic plane Oxz. The calculation shows that the main contribution to σ_{DCE} is that of collisions where the H_2 axis is parallel to Ox. The simplest way to understand this effect is to temporarily assume that the collision does not induce any momentum transfer between He and H_2, which means that (i) the orientation of the H–H axis axis is the same throughout the collision and (ii) the trajectory of the He atom is a straight line. In such conditions, when the turning point of the trajectory is reached, i.e., in the region where the $|1\rangle\rightarrow|2\rangle$ charge exchange can take place, the Jacobi γ angle is 0 if the initial orientation of H_2 is along the x axis, and $\pi/2$ if the initial orientation of H_2 is along either the y or z axis. As the coupling between the state $|1\rangle$ of symmetry $A'(A_1)\Sigma$ and the state $|2\rangle$ of symmetry $A'(B_2)\Sigma$ vanishes at $\gamma=\pi/2$, only the Ox orientation of H_2 can significantly contribute to the DCE cross section; then the H and H^+ fragments are deflected at 90° in the frame where H_2 is at rest, i.e., at large χ angle in the c.m. frame. Of course, the validity of the above interpretation relies on the validity of the assumption that there is no momentum transfer between He and H_2. One can see in Fig. 9(a) that this assumption is not strictly true, since the velocity of the center of mass of H_2 is smaller after the dissociation. Moreover, the analysis of the trajectories shows that there is a significant amount of rotational excitation of H_2. Nevertheless, despite the small impact parameter range

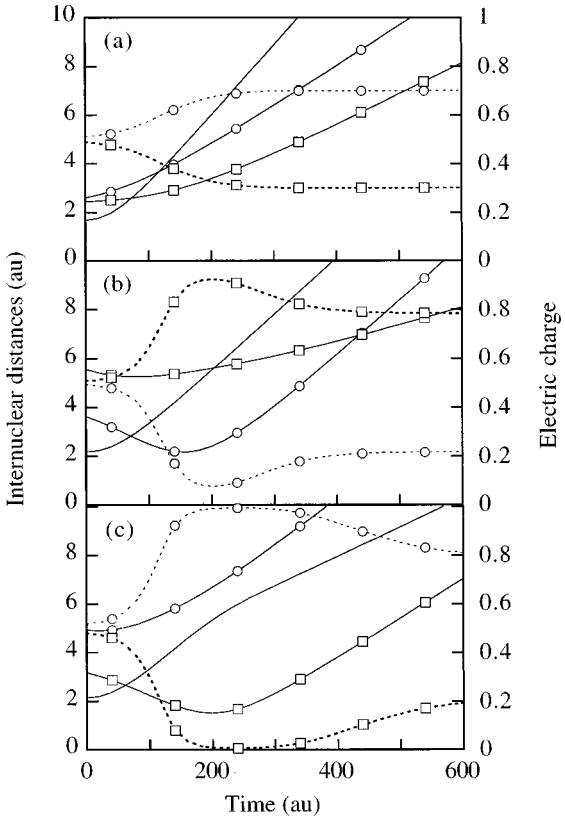

FIG. 10. Examples of time evolution of the second step of the DCE. The time $t=0$ corresponds to the transition between states 1 and 2.—, H_a-H_b r distance; —○—, He–H_a distance; —□—, He–H_b distance; --○--, electric charge of the H_a atom, which is zero for the neutral H atom and $+1$ for the H^+ ion; -□--, electric charge of the H_b atom. Frame (a): $E_{\text{coll}}=5$ eV, $v=0$; frames (b) and (c): $E_{\text{coll}}=5$ eV, $v=3$. The charge exchange between the two H atoms takes place at large r; the populations are not stabilized below $r<10$ a.u. In all cases, the charge is mainly carried by the H atom whose distance from the He atom is the largest as long as $r<10$ a.u.

which characterize the $v=0$ process [Fig. 5(a)], the momentum transfer between He and H_2 is certainly much weaker than the one we would have observed in a nondissociative process. As an illustration of this, one can note that the He atom is scattered in the forward direction [Fig. 9(a)]. This unusual feature is due to the dissociation of H_2; in the energy range studied here, this dissociation is so fast with respect to the collision motion that the H atoms are literally removed from the way of the He atom as soon as the $|1\rangle\rightarrow|2\rangle$ transition has taken place.

Another interesting point one can note in Fig. 9(a) is the asymmetry of the H and H^+ distributions for the $v=0$ DCE; relative to the initial H_2 direction, the H^+ ion is scattered primarily forward, while the neutral H atom is scattered primarily backward. Another effect of this disymmetry is that the H^+ ions are on average faster than the neutral H atoms. Statistical analysis shows that the relative He–H velocity is smaller than the relative He–H^+ velocity in nearly 70% of the $v=0$ $E_{\text{coll}}=5$ eV DCE collisions. This means that, although the H_2^+ ion is formed in its *ungerade* state with 50% of the electric charge on each of the H atoms, the charge is not equally shared at the end of the collision. Indeed, one sees in Fig. 10(a) that a charge transfer occurs between the H atoms at very large H–H separation; the electric charge on

the H atoms is not stabilized while r is less than about 10 a_0. The reason for that asymmetry has been given by Gislason and Guyon.[14] Because the helium atom is polarized by the electric charge, the collinear geometry of the ground HeH_2^+ state, namely the state $|3\rangle$, is $He–H^+–H$; the collinear geometry of the first excited HeH_2^+ state, namely the state $|2\rangle$, is $He–H–H^+$. This property also holds in noncollinear geometry: in the electronic state $|2\rangle$, the HeH^+ distance is larger than the HeH distance. Then, the electric charge is preferentially carried by the H atom which is the farthest from He as long as the H–H distance is smaller than 10 a_0, i.e., typically during the first 700 atomic units of time (a.u.t.) of the dissociation. Asymptotically, the distance r_a between He and H_a and the distance r_b between He and H_b can be approximated by

$$\begin{cases} r_a = r_a^0 + \dot{r}_a t \\ r_b = r_b^0 + \dot{r}_b t. \end{cases} \tag{23}$$

When $v=0$, the transition takes place at short internuclear distances, and r_a^0 and r_b^0 are small. Then, there is a strong correlation after 700 a.u.t. between $r_a > r_b$ and $\dot{r}_a > \dot{r}_b$ [Fig. 10(a)]. Consequently, the charge is carried by the H atom whose relative velocity with respect to the He atom is the largest.

At the same collision energy $E_{\text{coll}}=5$ eV, the doubly differential cross section $I(\chi,u)$ corresponding to $v=3$ [Fig. 9(b)] is different from that corresponding to $v=0$ [Fig. 9(a)]. Three main differences can be noted.

(a) In the frame where H_2 is initially at rest, the deflection angle distribution is more uniform in the $v=3$ case;
(b) The H and H^+ distribution are more symmetric;
(c) The He distribution is also in the forward direction, but is much broader. In a significant number of collisions, the He atom is faster than the incident H^+ ion.

As in the $v=0$ case, these results can be interpreted by assuming that there is no momentum transfer between He and H_2. For this long range process, the validity of such an impact parameter approximation is much better. Just as for $v=0$, the deflection angle distribution is closely related to the dependence of the DCE cross section with respect to the initial orientation of H_2. The calculation shows that the most efficient orientations are those where H_2 is initially in the Oxz plane. This is different from the $v=0$ situation, mainly because as the $|1\rangle \rightarrow |2\rangle$ transition can take place at large distance, any initial orientation of H_2 in the Oxz plane corresponds to a wide range of γ values in the transition region (while the Oy orientation corresponds to $\gamma=\pi/2$ throughout the collision). Then, the deflection angle distribution of H and H^+ reflects the initial orientation of the H_2 axis within the collision plane, i.e., is uniform in the frame where H_2 is initially at rest.

The same type of arguments can be invoked to explain the quasisymmetric distribution of the H and H^+ velocity vectors in the $v=3$ $E_{\text{coll}}=5$ eV case. The large internuclear distance for the $|1\rangle \rightarrow |2\rangle$ transition, together with the weakness of the momentum transfer between He and H_2, lead to the very simple result presented in Fig. 11; the location of the electric charge is mainly governed by the relative He–H positions at the transition time, and is not correlated with the final velocity as in the $v=0$ case.

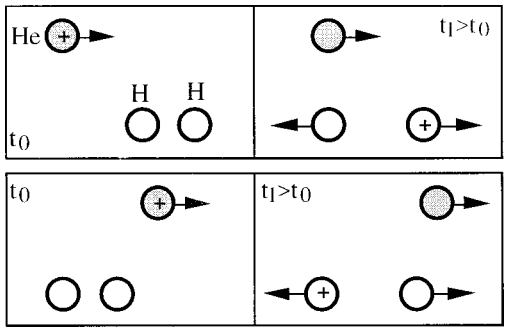

FIG. 11. Scheme of the time evolution of the positions of the nuclei in the impact parameter approximation, as seen in the frame where H_2 is at rest. In the upper view, the $|1\rangle \rightarrow |2\rangle$ transition takes place at $t=t_0$ before the turning point is reached. As the electric charge is carried by the H atom which is farthest from He at the beginning of the dissociation, the final relative $He–H^+$ velocity is small. Conversely, in the lower view, the $|1\rangle \rightarrow |2\rangle$ transition takes place after the turning point is reached. Then, the relative $He–H^+$ velocity is large.

Despite of its success in the interpretation of the $v=3$ results, the crude straight line trajectory model cannot account for some features observed in Fig. 9(b). The most spectacular one is the change in the velocity of the He atom; it is not very surprising to obtain a fraction of slow He atoms after the DCE. Indeed, although the main contribution to the cross section is due to large impact parameter collisions, the small impact parameters also contribute [Fig. 5(b)]. As seen in the $v=0$ case, these small impact parameter lead to the production of slow He atoms. More surprising is the production of a small amount of fast He atoms, i.e., faster than the incoming He^+ ion. This cannot be due to small impact parameter collisions, since these fast atoms are not produced by the $v=0$ collisions. These fast ions can be produced by collisions such as the one represented in Fig. 10(c), where the H_2 dissociation is followed by a He–H collision. Indeed, as the dissociation takes place preferentially in a plane, and as the dissociation velocity is larger than the collision velocity, the probability of such high energy He–H collisions is significant, which can result in an acceleration of the He atom.

IV. COMPARISON WITH OTHER WORK

A. Integral cross section

In the energy range 2–10 eV, two absolute measurements of the $v=0$ dissociative charge transfer (1) integral cross section[2,6,7] have been performed; they are quite different. As seen in Fig. 12, the presently reported cross sections is in much better agreement with the most recent results of Lehner *et al.*[6,7] than with those of Rozett *et al.*[2] The present results can also be compared to measured relative cross sections of Jones *et al.*[4] In Fig. 12, the latter data are scaled to the present results in the range 5–10 eV. The low energy results of Jones *et al.* were discarded in the scaling procedure, since they contradict the general trend of all measured low energy cross sections.[46–49] This calibration shows close

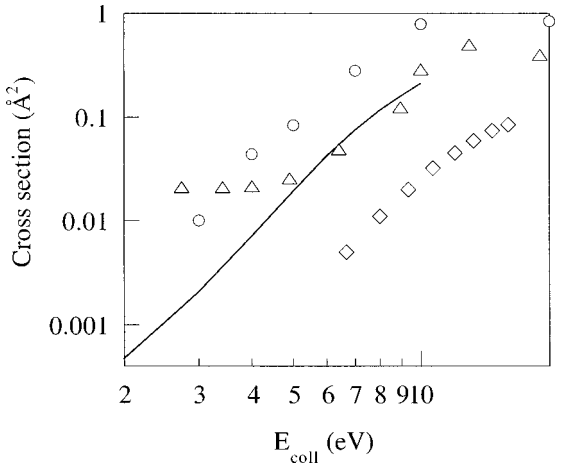

FIG. 12. Dissociative charge exchange cross section between He^+ and $H_2(v=0)$. Diamonds, Rozett *et al.* (Ref. 2); upward triangles, Jones *et al.* (Ref. 4) (these relative cross sections have been scaled to the theoretical results obtained in the range 5–10 eV); circles, Lehner *et al.* (Ref. 7); full line, this work.

agreement between these relative cross sections and the absolute cross sections measured by Lehner[6,7] and by Stedeford[1] at higher energy.

The present integral cross sections can also be compared with the previous ones[31] obtained using the frozen rotor approximation (Fig. 4). For the $v=0$ case, the frozen rotor approximation increases the cross section by a factor 2. This can probably be related to the fact that at very small internuclear distance where the charge exchange takes place, steric effects tend to orient the H_2 axis perpendicularly to the $He-H_2$ axis. As in the perpendicular geometry the coupling between states 1 and 2 vanishes, the cross section is smaller than the one obtained when the H_2 orientation is kept fixed. When v increases, the frozen rotor approximation becomes rather good; for $v=3$, freezing the rotation changes the cross sections by about 10% on the whole energy range studied here. Indeed, as the charge exchange takes place at large internuclear distance, steric effects do not play any role, and the rotation energy transferred to H_2 is not sufficient to change its orientation during the collision itself.

B. Differential cross section

Finally, the differential results can be compared with the measured energy spectra of the H^+ ion as a function of the H^+ scattering angle (Fig. 13). At each collision energy, the experimental data have been normalized to the present results. At $E_{coll}=4$ eV and 5 eV, theoretical and experimental results are in close agreement. The only noticeable discrepancy is the width of the energetic distribution at small angles α (below 80°) which is larger for the experiment than for the theory. This might be related to the width of the dissociation energy spectrum (Fig. 7), which is probably underestimated in the classical calculation of the second step of the DCE process. At $E_{coll}=7$ eV, the agreement is always good although the calculation fails to account for the experimentally observed structure at low energy, especially at small angle. At $E_{coll}=10$ eV, this low energy component becomes prominent in the experimental results, and the agreement is not good any more. To account for this discrepancy, one should probably consider another DCE channel,

$$He^+ + H_2 \rightarrow He + H^+ + H^*(n=2) \tag{24}$$

whose thermodynamical threshold is $E_{coll}=3.69$ eV. The assumption that this small energy-small angle structure is due to process (24) is qualitatively consistent with the description of the dynamics which has been done for process (1). Indeed, at moderate collision energy ($E_{coll}<10$ eV), the high lying states such those correlated to the $n=2$ levels of H can be reached at very small impact parameter only. Then, the $v=0$ dynamics of reaction (24) is more likely to be very similar to that of the $v=0$ reaction (1), except for two points. First, an important part of the collision energy goes into the electronic degree of freedom. Thus the H^+ ions formed by process (24) below 10 eV are expected to have a small velocity in the center of mass frame, i.e., to be peaked near the initial velocity of the He^+ ion in the laboratory frame. Second, the electronic states involved in the exit channel of (24) are correlated to $HeH^+(X\ ^1\Sigma^+)+H(n=2)$.[29] This means that the electric charge in collinear geometry will preferentially be carried by the intermediate H atom, which is exactly the contrary of what happens for reaction (1). This can explain why the energy of the H^+ ion formed by reaction (24) is so low; the high energy H atom does not carry any electric charge. This is also the reason of the increase of the energy of this H^+ ion with the detection angle, while the energy of the H^+ ions formed by reaction (1) increases when the detection angle decreases. This interpretation of the low energy component in the DCE spectrum below 10 eV is at variance with that proposed by Lehner,[7] which is based upon a vertical transition assumption, and assigns all the H^+ ions formed below 10 eV to reaction (1). Such a vertical transition assumption, which provides a nice description of the collision at high energy, is certainly questionable in the energy range studied here.

V. CONCLUSION

An angularly resolved theoretical treatment of the DCE process has been presented. Simultaneous use of two different dynamical methods have made it possible to treat each part of the collision with approximations enabling one to obtain differential results for this three body dissociation. When splitting the calculation into two distinct parts, the matching between these two parts is of course an important problem. In the present case, this is rather simple since multiple electronic transitions can be disregarded. The same approach would not give reliable results in strong coupling cases.

The dynamics of the title reaction is governed by the property that the electric charge can jump from He^+ to H_2 only in the immediate vicinity of the crossing seam. For the $v=0$ initial state of H_2, this means that the DCE process barely occurs unless the system explores the inner region, which is only possible at small impact parameter and high enough collision energy. Conversely, for the highly vibrationally excited H_2 ($v\geqslant 3$), the transition occurs mainly at a relatively large distance whatever the collision energy is.

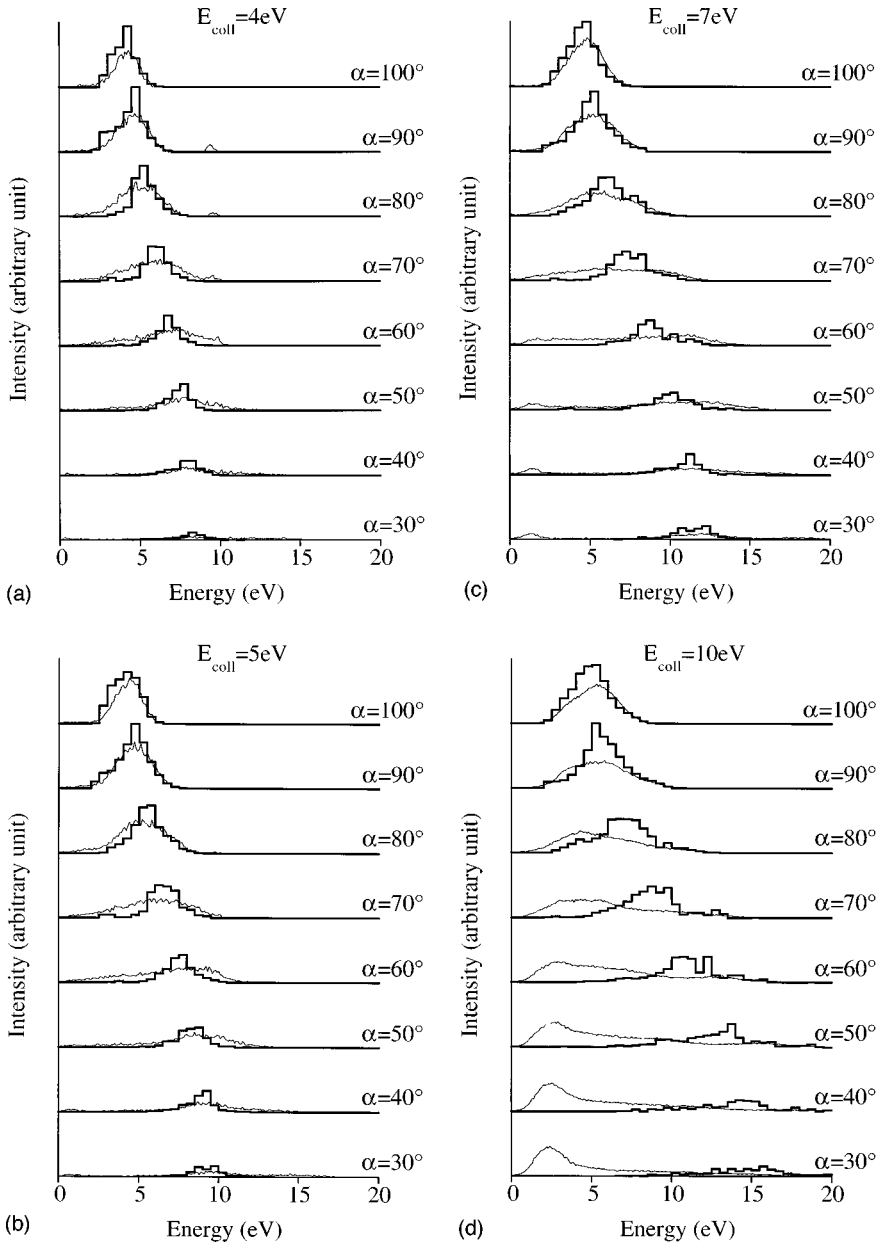

FIG. 13. Energy spectra of the H^+ ions produced by reaction (1) as a function of the collision energy E_{coll} and the angle α between the velocity of the H^+ ion and the initial velocity of the He^+ ion. The kinetic energy of H^+ and the deflection angle α are those obtained in the laboratory frame, where the H_2 molecule is initially at rest. The collision energy E_{coll} is the center of mass collision energy. The bold lines refers to the present calculation. The thin lines are the experimental results of Ref. 7.

This difference is the source of two different mechanisms, as observed either in the integral or in the differential cross sections. Finally, an important aspect of the dynamics is the localization of the electric charge on the H fragments, which can be understood using very simple arguments.

The comparison of mutually discrepant experimental results concerning the integral cross section with the present work is in favor of the most recent results performed by the group of Linder.[6,7] Besides, the agreement with the differential results obtained in the same group is very good for $E_{coll}<7$ eV. At $E_{coll}=10$ eV, the calculation fails to reproduce the experimental data. It is suggested that this discrepancy is related to the neglect of the highly excited states of the HeH_2^+ system, which can lead to production of excited H atoms. A further investigation is necessary to take into account these excited states, which are also responsible for the formation of HeH^+.

ACKNOWLEDGMENTS

I am very grateful to O. Lehner and F. Linder who provided me with a number of information concerning the experimental work they achieved at the Kaiserslautern University. I am indebted to A. Aguado, C. Suárez, and M. Paniagua, who allowed me to use their numerical code for computing the potential energy surfaces. Finally, it is a pleasure to thank V. Sidis and M. Sizun for very helpful discussions and advices.

[1] J. B. H. Stedeford and J. B. Hasted, Proc. R. Soc. London, Ser. A **227**, 466 (1955).
[2] R. W. Rozett and W. S. Koski, J. Chem. Phys. **48**, 533 (1968).
[3] T. F. Moran and R. J. Conrads, J. Chem. Phys. **58**, 3793 (1973).
[4] E. G. Jones, R. L. C. Wu, B. M. Hughes, T. O. Tiernan, and D. G. Hopper, J. Chem. Phys. **73**, 5631 (1980).
[5] D. G. Hopper and R. L. C. Wu, Chem. Phys. Lett. **81**, 230 (1981).
[6] O. Lehner, P. Reinig, and F. Linder, MOLEC X, 10th European Conference of Dynamics of Molecular Interaction, Salamanca, Spain, 1994 (unpublished).
[7] O. Lehner, thesis, University of Kaiserslautern, Germany, 1996.
[8] G. H. Dunn, R. Geballe, and D. Pretzer, Phys. Rev. **128**, 2200 (1962).
[9] B. Van Zyl, D. Jaecks, D. Pretzer, and R. Geballe, Phys. Rev. **158**, 29 (1967).
[10] R. A. Young, R. F. Stebbings, and J. W. McGowan, Phys. Rev. **171**, 85 (1968).
[11] G. N. Polyakova, V. A. Gusev, V. F. Erko, Y. M. Fogel, and A. V. Zats, Sov. Phys. JETP **31**, 637 (1970).
[12] R. C. Isler and R. D. Nathan, Phys. Rev. A **6**, 1036 (1972).
[13] P. Reinig, M. Zimmer, and F. Linder, *Nucl. Fusion A & M Suppl*. (IAEA, Vienna, 1992), Vol. 2, p. 95.
[14] E. A. Gislason and P. M. Guyon, J. Chem. Phys. **86**, 677 (1987).
[15] M. Sizun, G. Parlant, and E. Gislason, J. Chem. Phys. **88**, 4294 (1988).
[16] M. Sizun and E. Gislason, J. Chem. Phys. **91**, 4603 (1989).
[17] C. Edmiston, J. Doolittle, K. Murphy, K. C. Tang, and W. Wilson, J. Chem. Phys. **52**, 3419 (1970).
[18] P. J. Brown and E. F. Hayes, J. Chem. Phys. **55**, 922 (1971).
[19] P. J. Kuntz, Chem. Phys. Lett. **16**, 581 (1972).
[20] W. N. Whitton and P. J. Kuntz, Chem. Phys. Lett. **34**, 340 (1975); J. Chem. Phys. **64**, 3624 (1976).
[21] D. G. Hopper, Int. J. Quantum Chem., Symp. **12**, 305 (1978); J. Chem. Phys. **73**, 3289 (1980); **73**, 4528 (1980).
[22] F. Schneider and L. Zulicke, Chem. Phys. Lett. **67**, 491 (1979).
[23] R. Polák, J. Vojtík, I. Paidarová, and F. Schneider, Chem. Phys. **55**, 183 (1981); **76**, 259 (1983).
[24] C. Kubach, C. Courbin-Gaussorgues, and V. Sidis, Chem. Phys. Lett. **119**, 523 (1985).
[25] A. Russek and R. Furlan, Phys. Rev. A **39**, 5034 (1989).
[26] R. J. Furlan, G. Bent, and A. Russek, J. Chem. Phys. **93**, 6676 (1990).
[27] R. K. Preston, D. L. Thomson, and D. R. McLaughlin, J. Chem. Phys. **68**, 13 (1978).
[28] D. R. McLaughlin and D. L. Thompson, J. Chem. Phys. **70**, 2748 (1979).
[29] V. Sidis, Chem. Phys. **209**, 313 (1996).
[30] A. Aguado, C. Suárez, and M. Paniagua, J. Chem. Phys. **98**, 308 (1993).
[31] F. Aguillon, Chem. Phys. Lett. **222**, 69 (1994).
[32] J. P. Gauyacq and V. Sidis, Europhys. Lett. **10**, 225 (1989).
[33] F. Aguillon, V. Sidis, and J. P. Gauyacq, J. Chem. Phys. **95**, 1020 (1991).
[34] G. D. Billing, Comput. Phys. Rep. **1**, 239 (1984).
[35] V. Sidis in *State-Selected and State-to-State Ion-Molecule Reaction Dynamics, Part 2: Theory*, Advances in Chemical Physics Series, edited by M. Baer and C. Y. Ng (Wiley, New York, 1992) Vol. LXXXII, p. 73.
[36] M. A. Wartell and R. J. Cross, J. Chem. Phys. **55**, 4983 (1971).
[37] M. Sizun, D. Grimbert, and V. Sidis, Chem. Phys. Lett. **195**, 412 (1992).
[38] K. J. McCann and M. R. Flannery, J. Chem. Phys. **69**, 5275 (1978).
[39] A. E. DePristo, J. Chem. Phys. **79**, 1741 (1983).
[40] D. Kosloff and R. Kosloff, J. Comput. Phys. **52**, 35 (1983).
[41] R. Kosloff, J. Phys. Chem. **92**, 2087 (1988).
[42] C. Leforestier, R. H. Bisseling, C. Cerjan, M. D. Feit, R. Friesner, A. Guldberg, A. Hammerich, G. Jolicard, W. Karrlein, H.-D. Meyer, N. Lipkin, O. Roncero, and R. Kosloff, J. Comput. Phys. **94**, 59 (1991).
[43] S. Chapman in *State-Selected and State-to-State Ion-Molecule Reaction Dynamics, Part 2: Theory*, Advances in Chemical Physics Series, edited by M. Baer and C. Y. Ng (Wiley, New York, 1992), Vol. LXXXII, p. 423.
[44] M. E. Jones, S. E. Barlow, G. B. Ellison, and E. E. Ferguson, Chem. Phys. Lett. **130**, 218 (1986).
[45] V. Sidis and C. Courbin, Chem. Phys. **111**, 285 (1987).
[46] R. Johnsen and M. A. Biondi, J. Chem. Phys. **61**, 2112 (1974).
[47] R. Johnsen, A. Chen, and M. A. Biondi, J. Chem. Phys. **72**, 3085 (1980).
[48] H. Böhringer and F. Arnold, J. Chem. Phys. **84**, 1459 (1986).
[49] M. M. Schauer, S. R. Jefferts, S. E. Barlow, and G. H. Dunn, J. Chem. Phys. **91**, 4593 (1989).